Comprehensive Analysis of Bifurcation and Frequency Splitting Phenomena in Inductive Battery Charging Systems

Jiayu Zhou, C. Q. Jiang, *Senior Member, IEEE*, Tianlu Ma, *Graduate Student Member, IEEE*, Giuseppe Guidi, *Senior Member, IEEE*, Xinan Zhang, *Senior Member, IEEE*, and Jon Are Suul, *Member, IEEE*

***Abstract*—This article identifies the critical conditions of bifurcation and frequency splitting phenomena in inductive power transfer (IPT) systems used for battery charging, considering a constant voltage load (CVL) model. While prior studies covered these phenomena for IPT systems with constant resistance loads, their application to battery-loaded systems is limited due to the variation of equivalent load resistance with the operating frequency. By using the CVL model and analyzing the output power peak points, this article calculates the critical conditions for the frequency splitting phenomenon. This enables determining the power's monotonic range and peak in the frequency-control system. Moreover, by analyzing the monotonicity of the system's input impedance angle, the critical condition for bifurcation can be identified for determining the operating region that achieves zero-voltage switching or designing zero-phase angle IPT systems. To avoid bifurcation and achieve zero-voltage switching across the entire operational range, boundary conditions for frequency detuning design in systems with resistance or voltage loads are identified. The proposed analysis is validated through experimental measurements, and an example illustrating the impact of critical conditions on IPT system design for battery charging is provided.**

***Index Terms*—Bifurcation, critical condition, frequency splitting, inductive battery charging, zero voltage switching.**

Manuscript received 3 March 2024; revised 8 June 2024; accepted 14 July 2024. Date of publication 29 July 2024; date of current version 11 September 2024. This work was supported in part by the Science Technology and Innovation Committee of Shenzhen Municipality, China, under Grant SGDX20210823104003034, and in part by the Research Grants Council, Hong Kong SAR, under ECS Grant 21200622 and Grant CRF-YCRG C1002-23Y. Recommended for publication by Associate Editor G. Seo. *(Corresponding author: C. Q. Jiang.)*

Jiayu Zhou, C. Q. Jiang, and Tianlu Ma are with the Department of Electrical Engineering, State Key Laboratory of Terahertz and Millimeter Waves, City University of Hong Kong, Hong Kong, and also with the Joint Laboratory of Energy Saving and Intelligent Maintenance for Modern Transportations, Hong Kong (e-mail: jiayzhou@cityu.edu.hk; chjiang@cityu.edu.hk; tianlu.ma@my.cityu.edu.hk).

Giuseppe Guidi is with SINTEF Energy Research, 7034 Trondheim, Norway (e-mail: giuseppe.guidi@sintef.no).

Xinan Zhang is with the School of Electrical, Electronic, and Computer Engineering, University of Western Australia, Perth, WA 6009, Australia (e-mail: xinan.zhang@uwa.edu.au).

Jon Are Suul is with the Department of Engineering Cybernetics, Norwegian University of Science and Technology, 7034 Trondheim, Norway, and also with SINTEF Energy Research, 7034 Trondheim, Norway (e-mail: jon.a.suul@sintef.no).

Color versions of one or more figures in this article are available at https://doi.org/10.1109/TPEL.2024.3434620.

Digital Object Identifier 10.1109/TPEL.2024.3434620

I. Introduction

WIRELESS battery charging by inductive power transfer (IPT) technology is being utilized in diverse applications, including cell phones [1], electric vehicles [2], and marine transports [3]. In the design of IPT systems it is paramount to achieve high transfer efficiency and power capability. However, the occurrence of bifurcation and frequency-splitting phenomena, which has drawn considerable attention in the research community [4], [5], [6], [7], [8], [9], [10], [11], [12], [13], [14], can greatly impact these factors. Identifying the critical conditions for these phenomena is, therefore, of utmost importance.

To minimize the volt-ampere rating of sending-side components, IPT systems are typically designed to operate at the zero-phase angle (ZPA) condition. However, certain parameter conditions may cause multiple ZPA points to appear in the system characteristics, leading to the bifurcation phenomenon discussed in [4], [5], [6], and [7]. It is essential to establish the critical conditions for phase bifurcation when designing the system parameters and identifying feasible operating regions for ensuring zero voltage switching (ZVS). While previous literature has provided a criterion for ensuring a unique ZPA within various compensation topologies, this criterion is solely applicable to IPT systems with constant resistance load (CRL) [4]. In series–series (SS) compensated IPT systems, the bifurcation phenomenon tends to occur when increasing the coupling or the secondary side quality factor. This can significantly impact the operational limitations of the system, by resulting in potential issues such as the loss of ZVS or reduced efficiency in super-resonant frequency control [7]. To address these issues, the frequency detuning design of the resonant tank on both sides allows the system to operate without bifurcation for the entire load and coupling variations [7], [15], [18]. However, the corresponding boundary conditions for this frequency detuning design approach have not been provided in prior work.

While bifurcation is defined by the ZPA points of the input characteristics, the phenomenon of frequency splitting is associated with the output characteristics of IPT systems. Indeed, frequency splitting appears when the frequency characteristics of the power transferred to the load change from a single-peak curve to a double-peak curve [8], [9], [10], [11], [12], [13], [14]. This phenomenon has significant impact on the maximum power transfer capability and the interval where a monotonic

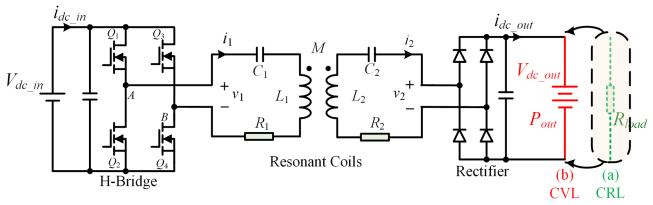

Fig. 1. SS-compensated IPT system with (a) CRL or (b) CVL.

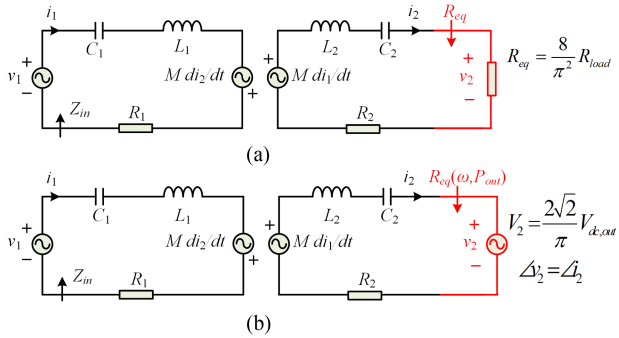

Fig. 2. Equivalent circuit of the SS-compensated IPT system using first harmonic approximation. (a) CRL cases. (b) CVL cases.

relationship between power and frequency is ensured. During frequency splitting-free operation, the system exhibits a wide power monotonic region, facilitating the design of a linear controller. In contrast, operation in frequency-splitting regions leads to the emergence of multiple power peaks and valleys. Thus, the frequency splitting phenomenon in IPT systems is important for defining the operating range and for facilitating the design of effective controllers. Critical conditions for when frequency splitting appears have been previously discussed in [8], but limited to IPT systems with CRL.

In various IPT applications, battery charging stands out as a common scenario. However, the equivalent resistance load of the battery varies significantly with output power and operating frequency, rendering inapplicable the critical conditions of bifurcation and frequency splitting phenomena derived on the assumption of a CRL. Therefore, it becomes necessary to reevaluate the frequency characteristics for systems designed with a battery load. Although the battery voltage changes gradually with the state-of-charge (SoC), the rate of change is extremely slow. In the time scale relevant for analyzing the steady-states and dynamics of high-frequency IPT systems, the battery voltage can be approximated as a constant voltage load (CVL) [23]. Considering this CVL model [18], this article derives the critical conditions for bifurcation and frequency splitting phenomena in SS-compensated inductive battery charging systems. Moreover, it is shown how a suitable frequency detuning design can be employed to both CVL and CRL to effectively avoid bifurcation across a wide range of load and coupling variations. The critical conditions associated with this approach are derived and presented.

The rest of this article is organized as follows. Section II provides an overview of the differences between bifurcation and frequency splitting, reviewing the boundary conditions for these phenomena with CRL. In Section III, the critical conditions for the bifurcation and frequency splitting phenomenon of IPT systems with CVL are presented. Section IV discusses the design of frequency detuning to avoid bifurcation in IPT systems with either CRL or CVL. Experimental results are presented in Section V. Finally, Section VI concludes this article.

II. Basis for Analysis of Bifurcation and Frequency Splitting Phenomenon

A. Differences Between CRL and CVL Systems

Fig. 1 illustrates a typical SS compensated IPT system, in which v_1 (v_2), i_1 (i_2), L_1 (L_2), C_1 (C_2), R_1 (R_2), and M denote the sending coil (pickup coil) voltage, current, inductance, capacitance, equivalent resistance, and mutual inductance, respectively. A diode rectifier is employed on the pickup side in terms of system cost, complexity, and power density. The figure displays two distinct load cases, CRL and CVL. CRL is represented by the dashed line, where R_{load} serves as the output load. Moreover, the commonly used scenario for battery charging is denoted by the solid line, with $V_{\text{dc\_out}}$ serving as the output voltage value. When using the first harmonic approximation [24], the equivalent circuits of systems with CRL and CVL are depicted in Fig. 2(a) and (b), respectively. This approximation assumes that only the fundamental components of ac voltage and current in the equivalent circuit need to be considered. In IPT systems that employ a CRL, the equivalent resistance can be easily determined and remains constant ($R_{eq} = 8R_{\text{load}}/\pi^2$). However, when dealing with IPT systems utilizing battery loads that can be equivalent to CVL, the situation is more complicated. In CVL systems with the diode rectifier, the amplitude of the load voltage v_2 remains constant ($|v_2| = 2\sqrt{2}V_{\text{dc\_out}}/\pi$), but the phase angle changes according to the load current i_2. Moreover, both the phase and amplitude of i_2 are influenced by the excitation frequency and sending voltage. As a result, the frequency characteristics of CVL systems cannot be accurately modeled using an equivalent CRL. While many studies have extensively covered the bifurcation and frequency splitting phenomena in CRL systems [4], [5], [6], [7], [8], [9], [10], [11], [12], [13], [14], the subsequent section reviews previous methods and conclusions that can serve as the basis for analyzing CVL systems.

B. Review of Bifurcation and Frequency Splitting Phenomenon of IPT Systems With CRL

In IPT systems, the occurrence of the bifurcation phenomenon is characterized by the presence of multiple ZPA frequency points, which provide valuable insights into the input characteristics and how they are influenced by different parameters. Based on the equivalent circuit shown in Fig. 2(a), the imaginary part of the input impedance of the CRL system can be obtained

$$\text{Im}(Z_{in}) = \omega L_1 - \frac{1}{\omega C_1} - \frac{(\omega L_2 - \frac{1}{\omega C_2})\omega^2 M^2}{(R_{eq}+R_2)^2 + \left(\omega L_2 - \frac{1}{\omega C_2}\right)^2}. \quad (1)$$

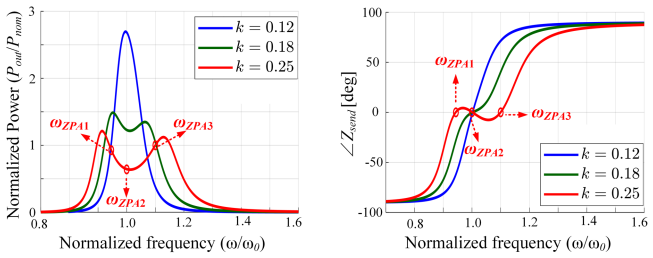

Fig. 3. Frequency characteristics and ZPA frequencies ($\omega_{\mathrm{ZPA}1}$, $\omega_{\mathrm{ZPA}2}$, and $\omega_{\mathrm{ZPA}3}$) of the IPT system with $Q_s = 5$. (a) Normalized output power versus frequency plot. (b) Input phase-angle versus frequency plot.

For the bifurcation phenomenon to appear, more than one solution of $\mathrm{Im}(Z_{\mathrm{in}}) = 0$ must be present. In such cases, the critical conditions can be calculated as [4], [5], [6], [7]

$$k > k_{\mathrm{bifurcation}} = \frac{1}{Q_s}\sqrt{1 - \frac{1}{4Q_s^2}} \approx \frac{1}{Q_s} \tag{2}$$

where k is the coupling coefficient and Q_s is the secondary side quality factor, defined as $k = \frac{M}{\sqrt{L_1 \cdot L_2}}$ and $Q_s = \frac{\omega_0 L_2}{R_2 + R_{eq}}$. The resonant frequency (ω_0) of both sides, is expressed as $\omega_0 = \frac{1}{\sqrt{L_1 C_1}} = \frac{1}{\sqrt{L_2 C_2}}$.

Moreover, the ZPA frequencies can be calculated by (2) [7], which is not described in this article due to space limitations. Equation (2) indicates that the bifurcation phenomenon is determined by k and Q_s, whereby large Q_s values or large k values make the system prone to bifurcation.

In contrast to the bifurcation phenomena, which appears in the input impedance, the frequency splitting phenomenon is defined by the output characteristics of the system. Indeed, frequency splitting appears when there is a change from one to two peaks in the output power characteristics. When the number of solutions for $\partial P_{\mathrm{out}}/\partial\omega = 0$ equals 3, it indicates that the system exhibits two power peaks and one power valley, which characterizes the presence of the frequency splitting phenomenon. Therefore, the critical conditions of frequency splitting within CRL systems can be calculated as [8]

$$k > k_{\mathrm{split}} = \sqrt{\frac{R_1^2 + (R_2 + R_{eq})^2}{2\omega_0^2 L_1 L_2}} \overset{L_1 = L_2}{\Rightarrow} k_{\mathrm{split}} \approx \frac{1}{\sqrt{2}Q_{\mathrm{s}}}. \tag{3}$$

The limits defined by (2) and (3) reveal different critical conditions for the bifurcation and frequency splitting phenomenon of IPT systems with CRL. For instance, for a CRL system with Q_s of 5, the critical coupling for the bifurcation phenomenon is approximately 0.2, while that of frequency splitting is about 0.14. Fig. 3 presents the frequency characteristic of the system under varying k values. The normalized power represents the power at the resonant frequency when $k = 0.2$. Notably, the bifurcation phenomenon does not occur at k values of 0.12 and 0.18, whereas the frequency splitting phenomenon occurs when the k value is 0.18. These results are consistent with (2) and (3), highlighting the divergence between bifurcation and frequency splitting phenomena. Moreover, multiple ZPA frequencies (ω_{ZPA1}, ω_{ZPA2}, and ω_{ZPA3}) of the system appear when bifurcation occurs at $k = 0.25$. The ZPA frequencies, ω_{ZPA1} and ω_{ZPA3}, do not align with the frequencies corresponding to the power peak. This inconsistency further demonstrates that bifurcation and frequency splitting represent distinct characteristics of the IPT system.

Previous studies have discussed these phenomena extensively in CRL systems and provided critical conditions [4], [5], [6], [7], [8], [9], [10], [11], [12], [13], [14]. For IPT systems with battery loads, the output load is often assumed to be equivalent to a pure resistance for steady-state analysis to simplify calculations [16], [17], but this approach is not suitable for analyzing frequency characteristics. In CVL systems, the equivalent R_{eq} value in (1) and (3) varies with the operating frequency, making it impossible to apply the results [i.e., (2) and (3)] obtained from frequency solutions and partial derivatives with respect to frequency to analyze these systems. Therefore, this article aims to analyze the bifurcation and frequency splitting phenomena in IPT systems with CVL.

III. Bifurcation and Frequency Splitting Phenomenon of IPT Systems With CVL

When considering an IPT system with the diode rectifier transferring power to a battery or a dc-bus with constant voltage, the equivalent circuit shown in Fig. 2(b) should be used to analyze the frequency characteristics of the system. It is worth noting that the battery can be approximated as a constant voltage source in series with a small equivalent resistance. Due to the negligible value of this equivalent resistance, the battery output voltage ($V_{\mathrm{dc\_out}}$) remains nearly constant across different charge and discharge currents [23]. Assuming the continuous conduction mode of the diode rectifier, the output voltage and current characteristics of the equivalent circuit load can be expressed as follows:

$$V_2 = \frac{2\sqrt{2}}{\pi} V_{\mathrm{dc\_out}} \tag{4}$$

$$\angle v_2 = \angle i_2. \tag{5}$$

When analyzing the steady state and dynamic behavior of IPT systems operating at high frequencies, the pickup voltage (V_2) of the equivalent circuit can be approximated as a CVL. In this case, an unbalanced factor, denoted as x_u, is defined as an indicator that reflects the balance ratio between the sending and pickup sides of the discussed IPT system

$$x_u = \sqrt{\frac{L_1}{L_2}}\frac{V_2}{V_1}. \tag{6}$$

Though the actual output power (P_{out}) of the system can be calculated based on the equivalent circuit and its output characteristics, the resulting expression is complicated and cannot be fully displayed due to space limitations. However, in the ideal case of lossless coils, the output power ($P_{\mathrm{out\text{-}lossless}}$) and input impedance angle (θ_{input}) of the system can be obtained, respectively [18] as follows:

$$P_{\mathrm{out-lossless}} = \frac{V_2^2\sqrt{\omega^2\left(\frac{k^2}{x_u^2} - 1\right) + 2\omega_0^2 - \frac{\omega_0^4}{\omega^2}}}{L_2\left(\omega^2(k^2 - 1) + 2\omega_0^2 - \frac{\omega_0^4}{\omega^2}\right)} \tag{7}$$

$$\theta_{\text{input}} = \arctan\left(\frac{(1-\frac{1}{x_u^2})+\frac{\omega_0^2}{\omega^2}(\frac{1}{x_u^2}-1)}{\sqrt{\frac{k^2}{x_u^2}-(1-\frac{\omega_0^2}{\omega^2})^2}}\right). \tag{8}$$

Based on (7), the operating frequency range of nonzero power transfer is derived as follows:

$$\max\left(\sqrt{\frac{\omega_0^2}{1+k/x_u}}, \sqrt{\frac{\omega_0^2}{1+k}}\right)$$

$$= \omega_{L1} < \omega < \omega_{H1} = \min\left(\sqrt{\frac{\omega_0^2}{1-k/x_u}}, \sqrt{\frac{\omega_0^2}{1-k}}\right). \tag{9}$$

Therefore, the operational region of the system is solely determined by k and x_u, with its expression varying based on whether x_u is greater or less than 1. Equations (7) and (8) provide lossless models that are valid within the frequency range described in (9). However, when considering R_1 and R_2, the actual operating frequency range of the IPT system is shown as follows:

$$\sqrt{\frac{\omega_0^2}{1+k/x_u}} = \omega_{L2} \le \omega \le \omega_{H2} = \sqrt{\frac{\omega_0^2}{1-k/x_u}}. \tag{10}$$

It is observed that when x_u is greater than 1, the operating frequency of the lossless model aligns with the actual system's operating frequency. However, when x_u is less than 1, the lossless model is not accurately representing the system behavior within $[\omega_{L2}, \omega_{L1}]$ and $[\omega_{H1}, \omega_{H2}]$. Therefore, the actual model of the system should be considered to obtain a comprehensive understanding of its characteristics in those frequency ranges.

A. *Critical Conditions of Bifurcation Phenomenon*

As noted earlier, the bifurcation phenomenon can be inferred by determining how many solutions exist within the working range where $\theta_{\text{input}} = 0$. However, analyzing the frequency characteristics of the system using the detailed model, which considers coil losses, can be excessively complex [18]. Instead, a simpler approach involves applying (7) and (8) derived from the lossless model for analysis within the operating frequencies $(\omega_{L1}, \omega_{H1})$. Moreover, the performance analysis of the detailed model within $[\omega_{L2}, \omega_{L1}]$ and $[\omega_{H1}, \omega_{H2}]$ will be considered to study the bifurcation characteristics of the system.

Fig. 4 illustrates the input impedance angle of the system for two different values of x_u. The blue dashed line represents the lossless model, which can be derived from (8). The red line segments correspond to the results calculated using the standard model, with Q representing the quality factor of coils. Moreover, the green data points are obtained from time-domain simulation results, which aligns nearly perfectly with the standard model results, exhibiting the same trends in the input impedance angle behavior. Notably, the lossless model exhibits remarkable accuracy within its designated frequency ranges $(\omega_{L1}, \omega_{H1})$. The partial derivative of the input impedance angle shown in (8) with respect to frequency can be calculated as follows:

$$\frac{\partial \tan(\theta_{\text{input}})}{\partial \omega} = \frac{2\omega_0^2 k^2 \omega^3 (x_u^2-1)}{x_u\left(k^2\omega^4 - x_u^2(\omega^2-\omega_0^2)^2\right)^{3/2}}. \tag{11}$$

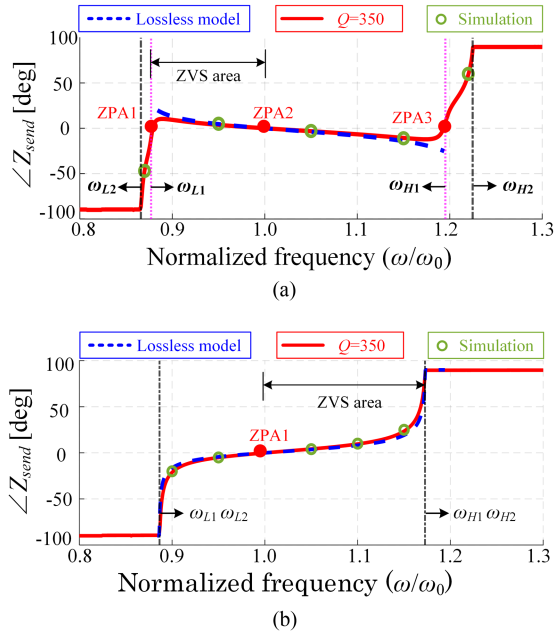

Fig. 4. Input impedance angle (θ_{input}) and ZPA points of IPT systems with CVL at $k = 0.3$. (a) $x_u = 0.9$. (b) $x_u = 1.1$.

This equation is limited to the frequency range $(\omega_{L1}, \omega_{H1})$, and the actual system's behavior should be considered in the ranges $[\omega_{L2}, \omega_{L1}]$ and $[\omega_{H1}, \omega_{H2}]$. Taking coil loss into account, the system operates purely capacitively at ω_{L2} and purely inductively at ω_{H2} [19]. Therefore, the input impedance angle of the actual system exhibits the following characteristics:

$$\underset{\omega\to\omega_{L2}}{Lim}\ \theta_{\text{input}} = -90^\circ; \theta_{\text{input}}(\omega=\omega_0) = 0^\circ; \underset{\omega\to\omega_{H2}}{Lim}\ \theta_{\text{input}} = 90^\circ. \tag{12}$$

When x_u is greater than 1, the behavior of the system throughout the entire operating frequency range can be determined using (10). In such cases, the input impedance angle exhibits a monotonically increasing trend because (11) consistently yields positive values. Consequently, the system will only have a ZPA point at $\omega = \omega_0$, which aligns with the observations in Fig. 4(b). When x_u is less than 1, (11) produces negative values, leading to a monotonically decreasing input impedance angle across the operating frequency range $(\omega_{L1}, \omega_{H1})$. In this scenario, the input impedance angle is greater than 0 at the ω_{L1} point and less than 0 at the ω_{H1} point. Moreover, the behavior of the system should be assessed based on the detailed model within the frequency range $[\omega_{L2}, \omega_{L1}]$ and $[\omega_{H1}, \omega_{H2}]$. According to (12), the system's impedance angle at ω_{L2} is -90°, indicating the presence of a ZPA point between ω_{L2} and ω_{L1}. Similarly, a ZPA point should also exist in the super-resonant frequency range. Therefore, the system would exhibit three ZPA points, as depicted in Fig. 4(a). Moreover, the critical condition for bifurcation to occur is that (11) must consistently yield negative results. This condition can be equivalently expressed as the following equation:

$$x_u < x_{u-\text{bifurcation}} = 1. \tag{13}$$

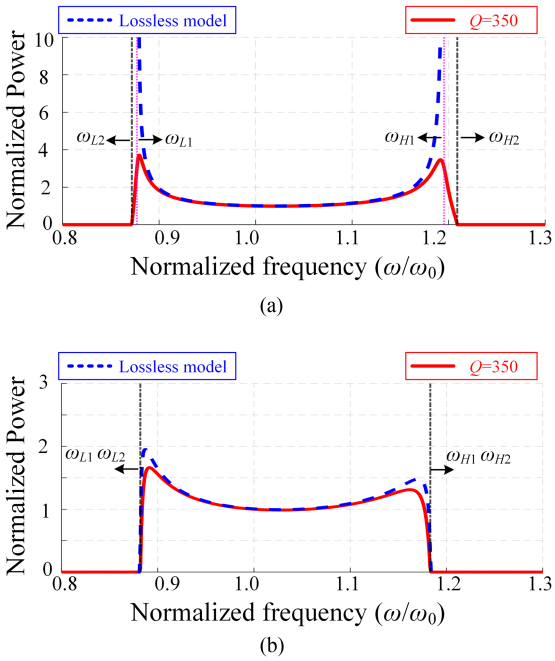

Fig. 5. Normalized output power and frequency splitting phenomenon of IPT systems with CVL at $k = 0.3$. (a) $x_u = 0.95$. (b) $x_u = 1.05$.

Unlike the CRL system, the bifurcation phenomenon of battery-loaded systems is not affected by k. Instead, it is determined by the unbalanced factor x_u. By controlling the input voltage v_1, bifurcation can be avoided in IPT systems with established output voltage and system parameters, making it easier to design the controller and operate within the desired area. Moreover, it is critical for the system to operate in soft switching conditions to ensure high performance. Identifying the bifurcation and ZPA points helps distinguish the soft switching range, which will be further elaborated later to calculate the critical conditions of ensuring ZVS throughout its entire operating range.

B. Critical Conditions of Frequency Splitting Phenomenon

The frequency splitting phenomenon is associated with the output characteristics of IPT systems, and appears when the system has two output power peaks. Analyzing the frequency splitting phenomenon of the system is crucial, as it helps assess the maximum power transfer capability and determine the region where its power transfer capability is monotonic with respect to frequency. Again, the lossless model, combined with the characteristics of the detailed model within the frequency range $[\omega_{L2}, \omega_{L1}]$ and $[\omega_{H1}, \omega_{H2}]$, is used to analyze the frequency splitting of the system.

Fig. 5 illustrates the output power of the IPT system at various x_u values. The blue dashed line represents the lossless model, which can be derived from (7). The red line segments correspond to the results calculated using the standard model, with Q representing the quality factor of coils. When $x_u<1$, according to (7), the output power of the lossless model exhibits a tendency toward positive infinity as the operating frequency approaches the boundary frequencies

$$\lim_{\omega\to\omega_{L1}} P_{\text{out-lossless}} = +\infty;\ \lim_{\omega\to\omega_{H1}} P_{\text{out-lossless}} = +\infty \quad (14)$$

This phenomenon occurs because R_1 and R_2 are disregarded, causing the input impedance to approach zero at the boundary frequencies. Therefore, the transferred power of the lossless system with a voltage load tends towards positive infinity. However, when considering R_1 and R_2, the power of a detailed IPT system model exhibits two peaks around the boundary frequencies due to the nonzero impedance, as illustrated in Fig. 5(a). Thus, the infinite value of the lossless system can be viewed as a power peak in the actual system. When x_u is less than 1, the lossless system must have two infinite power operating points at the boundary frequencies, as indicated by (7), implying that the actual system would also exhibit two output power peaks. Therefore, frequency splitting occurs in the system when x_u is less than 1.

When $x_u > 1$, the operating frequency range of the lossless system remains consistent with that of the actual system. Specifically, (9) is equivalent to (10) in this scenario. Therefore, the performance characteristics of the lossless IPT system closely resemble the detailed model, with a small error in the peak power, as depicted in Fig. 5(b). Moreover, (15) shown at the bottom of the next page, represents the partial derivative of (7) with respect to the operating frequency. Determining whether the system exhibits frequency splitting requires assessing the number of real roots of (15). By substituting $x = \omega^2$, the necessary and sufficient condition for (15) to be 0 is

$$f(x) = a \cdot x^4 + 4b \cdot x^3 + 6c \cdot x^2 + 4d \cdot x + e = 0 \quad (16)$$

where $a = (k^2-1)x_u^2 - k^4 + k^2$; $b = \frac{((-4k^2+2)x_u^2+2k^2)\omega_0^2}{4}$; $c = \frac{(3k^2x_u^2-3k^2)\omega_0^4}{6}$; $d = \frac{-2x_u^2\omega_0^6}{4}$; $e = x_u^2\omega_0^8$.

Equation (16) can be further processed and transformed into the following standard form:

$$f(y) = y^4 + p \cdot y^2 + q \cdot y + r = 0 \quad (17)$$

where $y = x + \frac{b}{a}$; $p = -\frac{6(b^2-ac)}{a^2}$; $q = \frac{4(a^2d-3abc+2b^3)}{a^3}$; $r = \frac{a^2(ae-4bd+3c^2)-3(b^2-ac)^2}{a^4}$.

By utilizing the Ferrari–Cardano derivation of the quartic formula [20], the distribution of the roots of (17) can be judged by

$$f(z) = z^3 + \frac{p}{2}z^2 + \frac{p^2-4r}{16}z - \frac{q^2}{64} = 0. \quad (18)$$

The condition that (17) has three or more distinct real roots is equivalent to the condition that (18) has three distinct real roots. Therefore, the IPT system satisfying the critical condition of frequency splitting can be judged by the roots of (18). According to the discriminant formula for cubic equations [21], the distribution of the root can be directly determined by (19) shown at the bottom of the next page. When the discriminant in (19) is greater than 0, it indicates that the original equation has three positive real roots. This implies that the system would exhibit frequency splitting. However, the root discriminant is quite complicated. Even if terms with small values can be ignored, it is difficult to obtain simple expressions showing the relationship between the frequency splitting

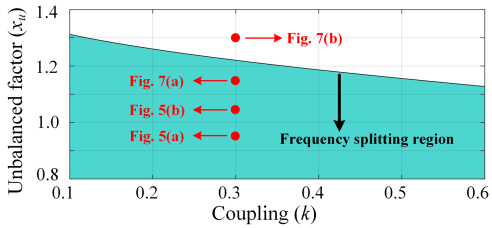

Fig. 6. Critical conditions of frequency splitting region of IPT systems with CVL.

phenomena and related parameters. However, the number of roots is only related to the coupling k and unbalanced factors x_u. Therefore, Fig. 6 can be obtained from (19), which directly indicates the frequency-splitting regions of the system under different couplings. Through polynomial curve fitting, the critical condition for frequency splitting phenomenon of IPT systems with CVL can be approximated and expressed as where $a_1 = \frac{p^2}{4} - \frac{3p^2-12r}{16}; b_1 = \frac{p(p^2-4r)}{32} + \frac{9q^2}{64}; c_1 = \frac{(p^2-4r)^2}{256} + \frac{3pq^2}{128}$

$$x_u < x_{u-\text{splitting}} \approx 0.4825k^3 + 0.7939k^2 - 0.7188k + 1.377. \tag{20}$$

Taking the case where k is equal to 0.3 in Fig. 7 as an example, the system has the frequency splitting phenomenon when x_u is 1.15, but the system does not have this phenomenon when x_u is 1.3. The simulation results (green data points) and standard model results (red line segments) are in line with the conclusions drawn in Fig. 6 and (20). Therefore, the critical conditions of the frequency splitting of the IPT system with CVL are demonstrated, which facilitates the design of the working area of the system and the corresponding controller.

IV. System Detuning Design and Critical Conditions for Avoiding Bifurcation

To maintain high performance in IPT systems, enabling soft switching of the converter on the sending side is crucial. Typically, the system operates within a super-resonant frequency range to achieve ZVS. However, the presence of bifurcation often limits the operable frequency range. To address these challenges, a frequency detuning factor, denoted as x_c in (21), is introduced to avoid bifurcation. This approach allows for a

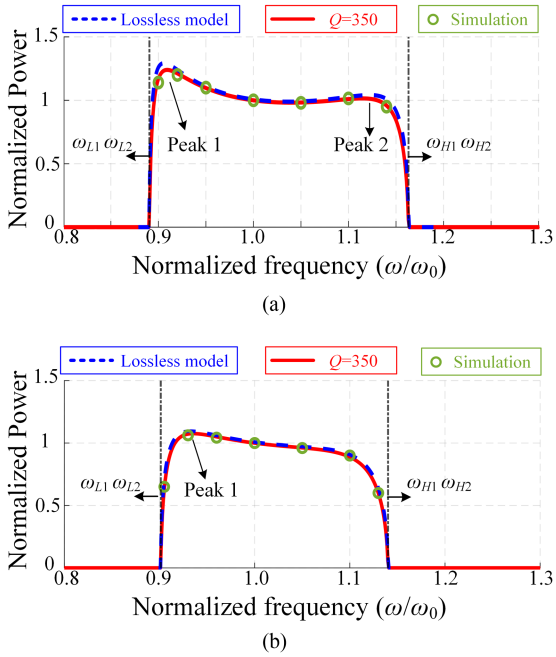

Fig. 7. Normalized output power of IPT systems with CVL at $k = 0.3$. (a) With frequency splitting phenomenon when $x_u = 1.15$. (b) Without frequency splitting phenomenon when $x_u = 1.3$.

wide operating range where ZVS can be achieved [7], [18]

$$x_c = \frac{C_1 L_1}{C_2 L_2}. \tag{21}$$

This method is applicable for both CRL and CVL scenarios. However, specific boundary conditions under different parameters are not explicitly provided. For nondetuned systems with a CRL, bifurcation phenomena occur when (3) is satisfied. By introducing x_c, the imaginary part of the system's input impedance, as shown in (2), can be further expressed as

$$\begin{aligned}\text{Im}(Z_{in}) = {} & (L_1L_2^2 - L_2M^2)\omega^6 \\ & + (L_1R_{eq}^2 + L_2M^2\omega_p^2 x_c - (1+2x_c)L_1L_2^2\omega_p^2)\omega^4 \\ & + (-L_1R_{eq}^2\omega_p^2 + (2x_c + x_c^2)L_1L_2^2\omega_p^4)\omega^2 \\ & - L_1L_2^2x_c^2\omega_p^6 = 0\end{aligned} \tag{22}$$

where ω_p is the resonant frequency of the sending side. The presence of bifurcation can be determined by examining the

$$\frac{\partial P_{\text{out-lossless}}}{\partial \omega} = \frac{((k^2-1)x_u^2 - k^4 + k^2)\omega^8 + \left((-4k^2+2)x_u^2 + 2k^2\right)\omega_0^2\omega^6 + (3k^2x_u^2 - 3k^2)\omega_0^4\omega^4 - 2x_u^2\omega_0^6\omega^2 + x_u^2\omega_0^8}{x_u\sqrt{-(\omega-\omega_0)^2(\omega+\omega_0)^2x_u^2 + k^2\omega^4}((k^2-1)\omega^4 + 2\omega_0^2\omega^2 - \omega_0^4)^2}. \tag{15}$$

$$\begin{aligned}\Delta_{\text{split}} = b_1^2 - 4a_1c_1 = {} & \frac{1}{256(k^4 - k^2x_u^2 - k^2 + x_u^2)^{12}}\Bigg(243\omega_0^{24}x_u^2k^6\Bigg(\left(\frac{1}{3}k^4 - \frac{4}{9}k^2 + \frac{16}{81}\right)x_u^{10} + \left(k^6 - \frac{32}{9}k^4 + \frac{88}{27}k^2 - \frac{32}{27}\right)x_u^8 \\ & + \left(-\frac{28}{9}k^6 + \frac{238}{27}k^4 - \frac{184}{27}k^2 + \frac{64}{27}\right)x_u^6 + \left(\frac{358}{81}k^6 - \frac{260}{27}k^4 + \frac{136}{27}k^2 - \frac{128}{81}\right)x_u^4 \\ & + \left(-\frac{28}{9}k^6 + \frac{43}{9}k^4 - \frac{4}{9}k^2\right)x_u^2 + k^6 - \frac{4}{3}k^4\Bigg)\Bigg)\end{aligned} \tag{19}$$

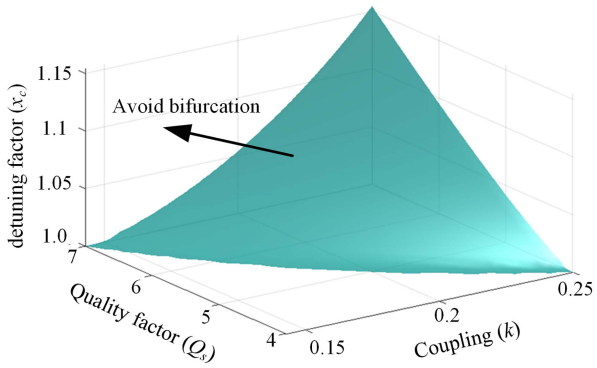

Fig. 8. Critical conditions for avoiding bifurcation of IPT systems with CRL obtained from (23).

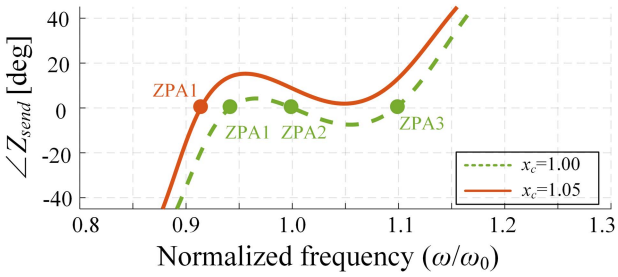

Fig. 9. Input impedance angles of an IPT system with CRL (k = 0.25, Q_s = 5) under different x_c.

number of ZPA frequency solutions in (22). The discriminant formula for equations, as shown in (23) shown at the bottom of this page, can be utilized to identify the occurrence of bifurcation phenomena. The bifurcation behavior of the system depends on the parameters x_c, k, and Q_s. By appropriately designing x_c, the system can avoid bifurcation for a given k and Q_s. However, the discriminant is complex, and obtaining the boundary conditions for designing x_c to avoid bifurcation is facilitated through graphical analysis, as depicted in Fig. 8. For instance, considering k = 0.25 and Q_s = 5, setting x_c to a value greater than 1.042 can prevent bifurcation. This is demonstrated in Fig. 9, which depicts the input impedance angle of the system when x_c is 1.05. The system successfully avoids the bifurcation phenomenon, confirming consistency with the calculated results.

Moreover, it is imperative to discuss the critical condition for avoiding bifurcation in IPT systems with CVL. When x_u exceeds 1, the system is free from bifurcation phenomena and typically operates within the super-resonant frequency range to achieve ZVS. However, x_u can also be designed to be less than 1 to greatly increase the output power capability, which leads to system bifurcation [18]. Indeed, x_c slightly higher than 1 can be introduced in the system to avoid bifurcation and

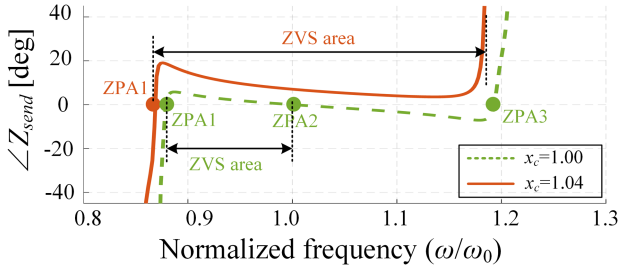

Fig. 10. Input impedance angles of an IPT system with CVL (k = 0.3, x_u = 0.95) under different x_c.

achieve ZVS within the working range, as depicted in Fig. 10 [18]. However, specific critical conditions are not provided in previous literature. When considering the introduction of x_c, the input impedance angle of the system can be calculated using the following equation:

$$\theta_{\text{input}} = \arctan\left(\frac{(1-\frac{\omega_p^2}{\omega^2})-\frac{1}{x_u^2}(1-\frac{x_c\cdot\omega_p^2}{\omega^2})}{\sqrt{\frac{k^2}{x_u^2}-(1-\frac{\omega_p^2}{\omega^2})^2}}\right). \tag{24}$$

The denominator in (24) is always greater than 0. Hence, the inductive input impedance can be achieved by satisfying the following conditions:

$$x_c \geq \frac{\omega^2}{\omega_p^2}\cdot\left(1-x_u^2+\frac{\omega_p^2}{\omega^2}x_u^2\right). \tag{25}$$

In the frequency range $(\omega_{L1}, \omega_{H1})$, (24) exhibits a monotonically decreasing behavior. Therefore, the boundary conditions to avoid bifurcation can be obtained by substituting the boundary frequency ω_{H1} into (25) as follows:

$$x_c \geq \frac{kx_u^2-1}{k-1}. \tag{26}$$

This serves as a critical condition to prevent bifurcation across the full frequency range. A flowchart shown in Fig. 11 helps determine whether the IPT system will exhibit the bifurcation phenomenon. This flowchart also guides the design of the x_c to effectively avoid bifurcation. Moreover, the flowchart provides information about the region where ZVS can be realized in the system.

LTspice simulations are also included to verify these analytical results. Fig. 12 presents the simulation results for different values of x_c at 100 kHz. When x_u is less than 1, the input impedance angle of the system exhibits a monotonic decrease within the frequency range $(\omega_{\text{L1}}, \omega_{\text{H1}})$, indicating the occurrence of bifurcation. In this case, the system loses ZVS in the main

$$\begin{aligned}\Delta_{avoid\_bif} = &-(Q_s^8k^4+2Q_s^6k^2-4Q_s^6+Q_s^4)x_c^4-(4Q_s^8k^6-2Q_s^8k^4+10Q_s^6k^4-26Q_s^6k^2+16Q_s^6+8Q_s^4k^2-12Q_s^4+2Q_s^2)x_c^3\\&-(Q_s^8k^4-22Q_s^6k^4+46Q_s^6k^2+Q_s^4k^4-24Q_s^6-18Q_s^4k^2+22Q_s^4+2Q_s^2k^2-8Q_s^2+1)x_c^2\\&-(-22Q_s^6k^2+16Q_s^6+22Q_s^4k^2-12Q_s^4-4Q_s^4k^2+2Q_s^2)x_c+4Q_s^6-Q_s^4\end{aligned} \tag{23}$$

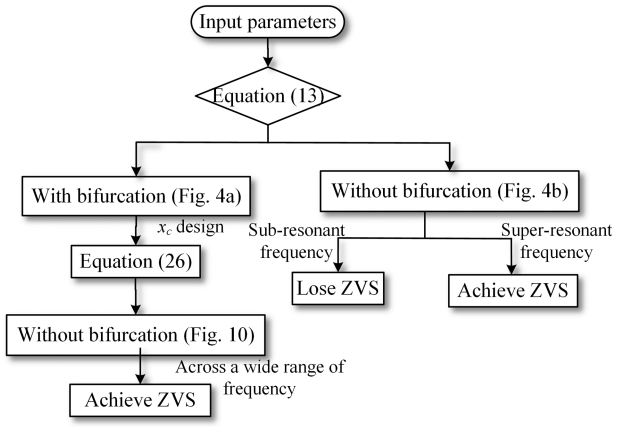

Fig. 11. Design flowchart of x_c to avoid bifurcation and determination of ZVS area in IPT systems with CVL.

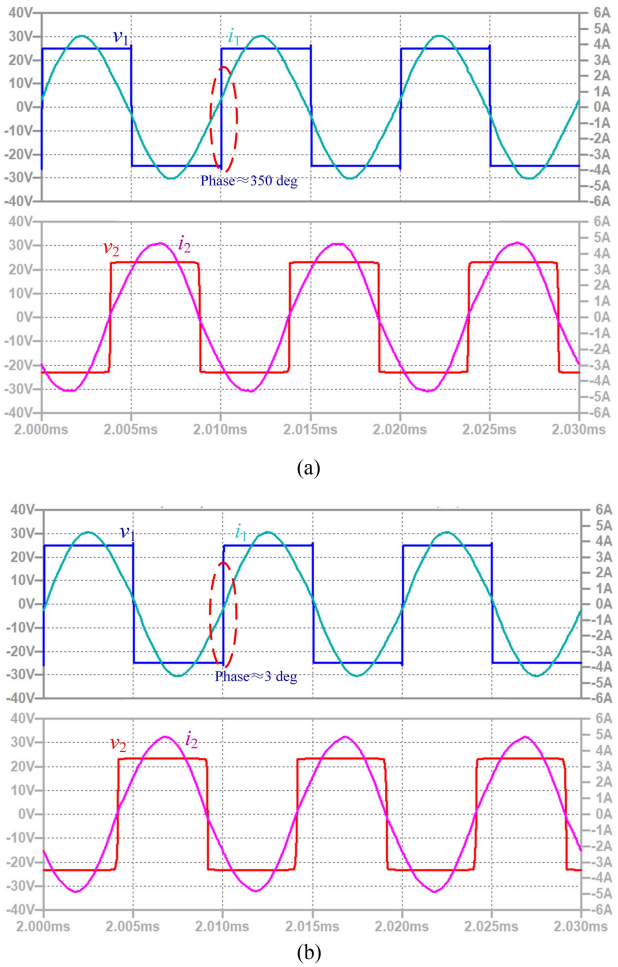

Fig. 12. LTspice simulation waveforms of the IPT system with CVL ($k = 0.35$, $x_u = 0.95$) operating at 100 kHz under different x_c. (a) $x_c = 1$. (b) $x_c = 1.05$.

super-resonant frequency region, as shown in Fig. 4(a). By designing the system based on the expression for x_c provided in (26), the LTspice simulation results shown in Fig. 12(b) demonstrate that the input impedance angle of the system remains close to 0. This outcome is consistent with the analytical calculations.

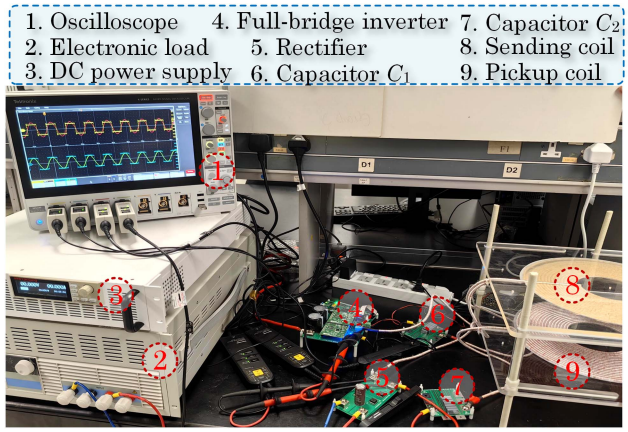

Fig. 13. Prototype of the IPT system.

TABLE I
PARAMETERS OF THE IPT-SYSTEM

General parameters	Values
Input voltage, V_{dc_in}	25 V
Output voltage, V_{dc_out}	20–35 V
Self-inductance, L_1, L_2	57, 57 μH
Mutual inductance	9–20 μH
pickup coil resonant frequency, f_0	85.0 kHz
Quality factor, Q_1, Q_2	350, 350
Semiconductor devices of H-bridge	EPC 2022
Diodes of rectifier	SBM3060VDC-AU_R2_006A1

The need to avoid bifurcation in IPT systems is application-dependent. For frequency-control IPT systems [7], avoiding bifurcation can significantly expand the ZVS operating region, as shown in Fig. 10. This results in a slight improvement in system efficiency in the super-resonant frequency region. However, avoiding bifurcation is not always necessary. For instance, in some ZPA-controlled IPT systems, bifurcation is desirable to achieve high misalignment tolerance and constant efficiency [25]. Therefore, the selection of the parameter x_c, which plays a crucial role in avoiding bifurcation phenomena, is dependent on the system parameters and may impact overall performance. When designing x_c, it is advisable to consider both bifurcation avoidance and achieving ZVS within the desired operating range. Taking the example of CVL systems, the boundary frequencies of the intended operating range can be substituted into (25) to determine the appropriate value of x_c. This enables soft switching and ensures the prevention of bifurcation throughout the targeted operating range. By following this approach, the value of x_c tends to be closer to 1, minimizing its influence on other system characteristics and performance.

V. Experimental Results

To verify and illustrate the comprehensive analysis of bifurcation and frequency splitting phenomena in IPT systems, a laboratory prototype is constructed, as shown in Fig. 13. The system specifications are listed in Table I. In the experiment, the resonant tank was designed based on a resonant frequency of 85 kHz. Since the voltage level does not significantly impact

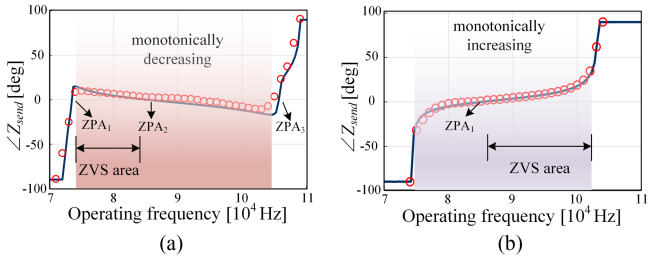

Fig. 14. Input impedance angles of the IPT system with CVL ($k = 0.35$) under different x_u. (a) $x_u = 0.9$. (d) $x_u = 1.1$.

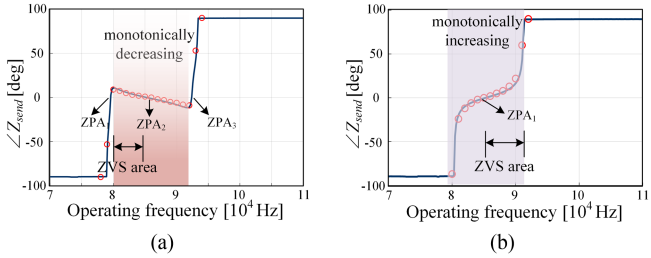

Fig. 15. Input impedance angles of the IPT system with CVL ($k = 0.15$) under different x_u. (a) $x_u = 0.9$. (b) $x_u = 1.1$.

these phenomena, an input voltage of 25 V was selected to prevent overcurrent, as the system may operate at nonresonant frequency points. The MOSFET used in the inverter is a GaN device, model EPC 2022. The diode rectifier employed on the receiving side is the SBM3060VDC-AU_R2_006A1. The design of the coils is identical on both the sending and receiving sides. They are spiral coils with 17 turns, an inner diameter of 10 cm, and an outer diameter of 28 cm. Moreover, a dc power supply is employed on the input side to provide power and allows for the adjustment of the input voltage, enabling the system to operate at different x_u values. On the output side, an electronic load is connected to simulate the behavior of either a CVL or CRL.

A. Verification of Critical Conditions for the Bifurcation Phenomenon

Fig. 14 presents the input impedance angle of the system for various x_u values at $k = 0.35$. The solid line represents the theoretical results, while the dots indicate the experimental results. The agreement between the model and experimental data is observed to be excellent in the core frequency region. Although slight discrepancies are noticed near the boundary frequency, the general trend of the impedance angle remains consistent. Bifurcation phenomena are observed in the system when x_u is less than 1, aligning with the theoretically computed boundary conditions shown in (13). In IPT systems with CVL, the critical condition of bifurcation phenomena also aids in identifying the regions where soft switching can be ensured. Specifically, when x_u is less than 1, the subresonant frequency range becomes the region for potential soft switching, while for x_u greater than 1, soft switching can be realized in the super-resonant frequency range.

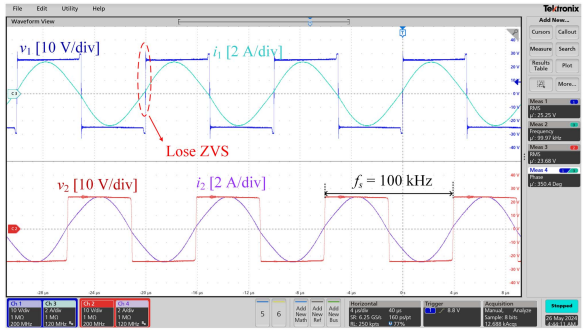

Fig. 16. Waveforms of the IPT system with CVL ($k = 0.35$) operating at 100 kHz under different x_u. (a) $x_u = 0.95$ ($P_{\text{out}} = 70$ W; $\eta = 93.3\%$). (b) $x_u = 1.05$ ($P_{\text{out}} = 69$ W; $\eta = 94.6\%$).

Fig. 15 presents the low coupling results with $k = 0.15$, which verify the critical conditions governing the frequency bifurcation phenomenon. It can be observed that when the unbalanced factor x_u is less than 1, the system exhibits the bifurcation characteristic, presenting three ZPA points. Conversely, when x_u is greater than 1, the system has only a single ZPA point, indicating the absence of bifurcation. There experimental findings are fully consistent with the calculated critical conditions presented in (13). Therefore, the critical condition for frequency bifurcation of IPT systems with CVL is determined solely by the parameter x_u, and is not affected by the coupling coefficient.

Fig. 16 presents the waveforms of the system at 100 kHz to showcase the impact of different values of x_u. When x_u is less than 1, the system exhibits a monotonically decreasing behavior in this frequency range, demonstrating inductive input characteristics and achieving soft switching. Conversely, when x_u is greater than 1, the system indicates capacitive input characteristics resulting in hard switching. These experimental results align well with the theoretical analysis and experimental results in Fig. 14.

B. Verification of Critical Conditions for the Frequency Splitting Phenomenon

The experimental results of output power of the system for different x_u values at $k = 0.35$ are displayed in Fig. 17. For $x_u = 1.15$, the system exhibits a distinct power peak in the subresonant region. As the operating frequency increases within the sup-resonant frequency region, a slight power increase is

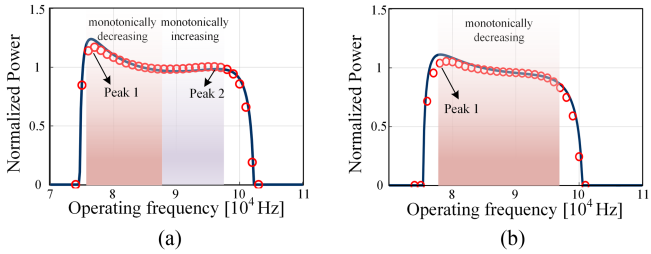

Fig. 17. Normalized output power of the IPT system with CVL ($k = 0.35$, $x_{u\text{-critical}} = 1.2$) under different x_u. (a) $x_u = 1.15$. (b) $x_u = 1.25$.

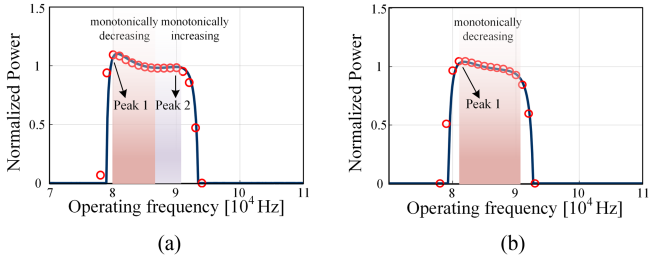

Fig. 18. Normalized output power of the IPT system with CVL ($k = 0.2$, $x_{u\text{-critical}} = 1.26$) under different x_u. (a) $x_u = 1.2$. (b) $x_u = 1.3$.

observed near the upper boundary frequency, leading to the presence of another power peak. Therefore, the system experiences frequency splitting. Conversely, when x_u is set to 1.25, the system displays a single power peak solely in the subresonant frequency region. As the operating frequency rises, the system's power gradually decreases, indicating the absence of the frequency splitting phenomenon. These observations align with the theoretical results shown in (20), where $x_u = 1.2$ corresponds to the critical condition of the system with $k = 0.35$. Moreover, Fig. 18 illustrates the experimental results of different x_u values with k of 0.2. Notably, When the unbalanced factor x_u falls below the calculated critical x_{u_critical}, the system exhibits frequency splitting. In contrast, when x_u exceeds the $x_{u\text{-critical}}$, the system avoids frequency splitting. Investigating the presence of frequency splitting provides valuable insights into the power peaks and the monotonic behavior of output power, facilitating the selection of operating regions and the design of controllers.

C. Verification of Critical Conditions for the Detuning Design for Avoiding Bifurcation

To verify the calculation of the critical conditions of frequency detuning, Fig. 19 shows the input impedance angle of the system under different x_c. When x_c equals 1, the system exhibits a bifurcation phenomenon due to x_u being less than 1. To avoid this phenomenon, x_c can be calculated to be approximately 1.05 using (26). By setting x_c to this value, the system possesses one ZPA point only in the subresonant frequency region, effectively avoiding frequency bifurcation, as depicted in Fig. 19. In this case, the system can significantly expand the ZVS operating region shown in Fig. 19. Moreover, Fig. 20 displays the waveforms of the system operating at 100 kHz with different x_c values. It can be observed that the input impedance angle of the original system is $-9.5°$. Following the calculated

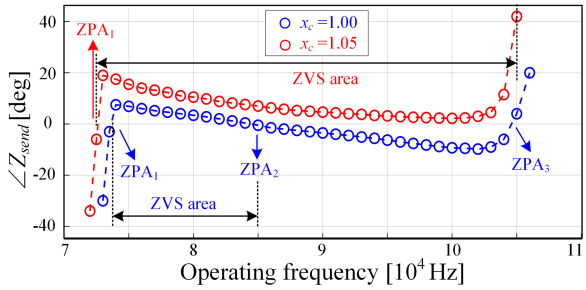

Fig. 19. Input impedance angle of the IPT system with CVL ($k = 0.35$, $x_u = 0.95$) under different x_c.

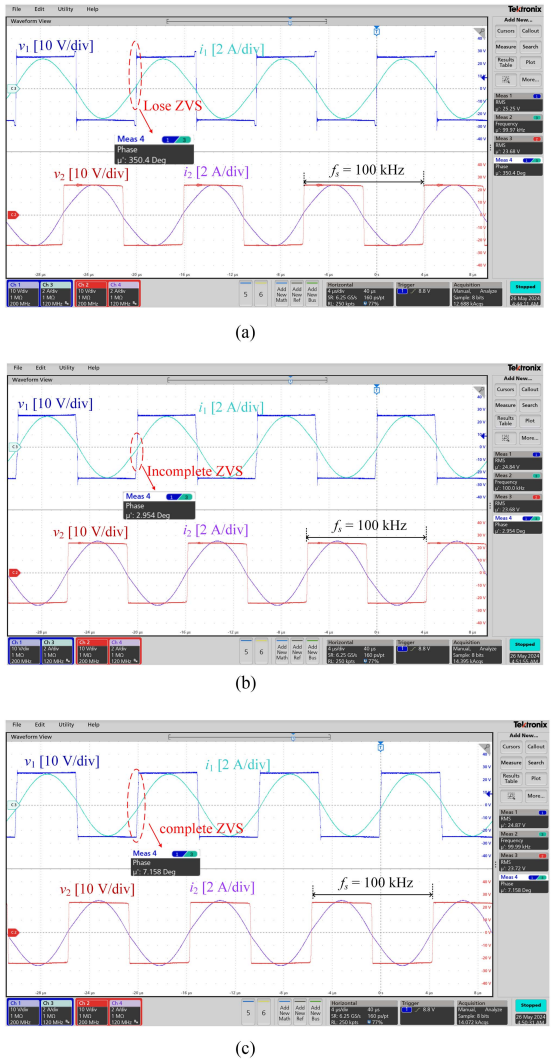

Fig. 20. Waveforms of the IPT system with CVL ($k = 0.35$, $x_u = 0.95$) operating at 100 kHz under different x_c. (a) $x_c = 1$; ($P_{\text{out}} = 70$ W; $\eta = 93.3\%$). (b) $x_c = 1.05$ ($P_{\text{out}} = 74$ W; $\eta = 93.8\%$). (c) $x_c = 1.065$ ($P_{\text{out}} = 74$ W; $\eta = 93.9\%$).

frequency detuning design, the input impedance angle of the system closely approaches 0 shown in Fig. 20(b), aligning with the calculated critical detuning results. It is worth noting that the input impedance angle is not precisely 0, which may be attributed to factors such as parasitic parameters of the device. Therefore, the designed frequency detuning approach enables

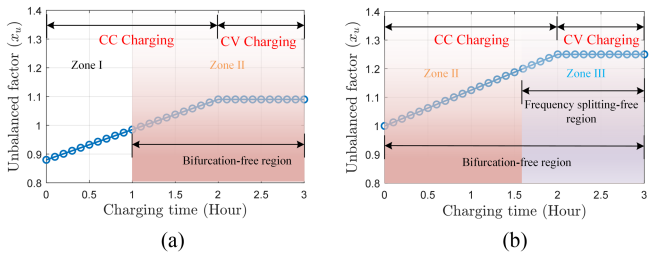

Fig. 21. Variation of unbalanced factors in IPT systems with $k = 0.35$ during battery charging (battery voltage range: 150–185 V [22]). (a) System I: Input voltage of 170 V. (b) System II: Input voltage of 150 V.

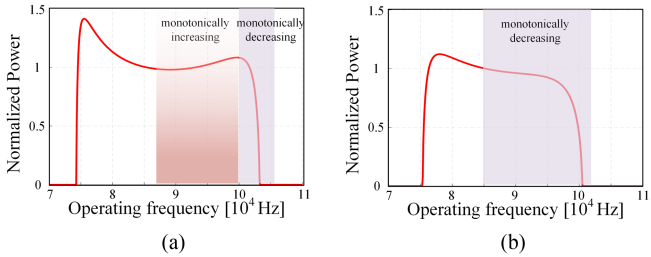

Fig. 22. Relationship between normalized output power and operating frequency in CV charging mode. (a) System I. (b) System II.

the system to evade bifurcation across a wide frequency range. The critical x_c, as indicated in (26), generally aligns with the experimental results. It is worth noting Fig. 20(b) shows the system achieves incomplete soft switching due to the input impedance angle being close to 0°. To realize complete soft switching, it is desirable for the MOSFET voltage to approach zero before turn-ON, which can be accomplished by ensuring negative inductor current (I_1) to discharge the parasitic output capacitance [26]. Therefore, by further slightly increase x_c, the operation can be transitioned from the incomplete ZVS state to a complete ZVS state, as illustrated in the improved waveforms of Fig. 20(c).

D. Example of Utilizing Identified Critical Conditions for Inductive Battery Charging Design

Battery charging is a common IPT application, and the direct connection to the battery terminals will impose CVL characteristics of the system model. However, the battery voltage depends on the SoC, which implies that the output voltage will change slowly during the charging process. Depending on the battery chemistry, the battery voltage can vary within a specified range defined by the voltages at minimum and maximum SoC. As an example, the voltage range of 150–185 V presented in [22] is utilized in the following. Figs. 21 and 22 illustrate the implication of two different system designs when considering the conventional intervals of constant current (CC) and constant voltage (CV) charging. In system I, the input dc voltage is set at 170 V, while in system II, it is set at 150 V. In Zone I of Fig. 21, the system exhibits both bifurcation and frequency splitting phenomena; in Zone II, the system avoids bifurcation but still exhibits frequency splitting; and in Zone III, neither bifurcation nor frequency splitting occurs in the system.

During charging, the battery voltage increases slowly, resulting in variation of unbalanced factors x_u within the IPT system, as depicted in Fig. 21. In the CC mode, as the battery voltage increases, the system unbalanced factor x_u continues to rise. System I exhibits the bifurcation phenomenon in the early stages, whereas system II maintains an unbalance factor x_u greater than 1, thus avoiding bifurcation throughout the process. Moreover, when the battery enters the CV mode, the charging power of the battery needs to be significantly attenuated due to the reduced charging current [22]. However, system I remains in the frequency-splitting region, making it challenging to achieve low output power by controlling operating frequencies since the output power of the system does not consistently change monotonically with the frequency, as depicted in Fig. 22(a). In contrast, system II successfully avoids the frequency-splitting phenomenon in CV mode. Fig. 22(b) demonstrates the output power curve corresponding to operating frequency changes. By simply adjusting the operating frequencies in the super-resonant frequency region, low-power charging in CV mode can be achieved in system II. Therefore, the analysis presented in this article enables quick and easy identification of these regions and system characteristics, facilitating the design and optimization of system parameters and controllers in IPT systems with battery loads.

E. Comparison With Existing Literature

While previous studies [4], [5], [6], [7], [8], [9], [10], [11], [12], [13], [14] have focused on investigating the bifurcation and frequency splitting phenomena in IPT systems with CRL, we have addressed a research gap by considering IPT systems with battery loads, which can be approximated as a CVL. This distinction is significant due to the increasing use of battery charging applications, prompting a reevaluation of the bifurcation and frequency splitting phenomena in IPT systems. The CVL model shown in (7)–(8) utilized in this article is based on the findings of [18]. While the model itself remains the same, the research questions addressed in this article are distinct. In [18], the focus is on designing subresonant frequency control using the CVL model. In contrast, this article comprehensively explores the bifurcation and frequency splitting phenomena in IPT systems based on the CVL model. To highlight the distinctions between this article and previous literature, Table II has been included to provide a detailed comparison between this manuscript and existing methods, emphasizing the unique contributions of this work. In fact, analyzing the critical conditions governing these frequency-dependent phenomena can provide valuable insights to optimize system design and control, as demonstrated across various CRL system case studies [4], [5], [6], [7], [8], [9], [10], [11], [12], [13], [14]. Therefore, further investigation of these phenomena in voltage-loaded systems can offer crucial guidance for the system design and control design, especially for frequency-controlled systems and ZPA-controlled systems with CVL [25]. Moreover, when avoiding bifurcation is desirable [7], the boundary conditions of x_c are calculated in this article to achieve this goal, for both CRL and CVL scenarios.

TABLE II
COMPREHENSIVE INVESTIGATION OF FREQUENCY BIFURCATION AND FREQUENCY SPLITTING PHENOMENA IN IPT SYSTEMS

References	Load type	Critical conditions for bifurcation	Critical conditions for frequency splitting	x_c design for avoiding bifurcation
[4], [5], [6]	CRL	For CRL systems	N/A	N/A
[8], [9], [10], [11], [12], [13], [14]	CRL	N/A	For CRL systems	N/A
[7]	CRL	For CRL systems	N/A	Larger than 1 for CRL system
[18]	CVL	N/A	N/A	Slightly larger than 1 for CVL system
This article	CVL	(13) for CVL systems	(20) for CVL systems	(23) for CRL systems (26) for CVL systems

VI. CONCLUSION

This article presents a comprehensive analysis of bifurcation and frequency splitting phenomena in IPT systems with CVL. The critical conditions for these phenomena are examined and compared to IPT systems with CRL. The article reveals that the bifurcation phenomenon occurs in the system with CVL when the unbalance factor x_u is less than 1, regardless of the coupling coefficient k. Moreover, the critical condition of frequency splitting phenomenon for IPT systems incorporating CVL has been computed. The findings reveal that the frequency splitting phenomenon occurs when the unbalance factor x_u is large, with the boundary value increasing as system coupling k decreases. This article also provides boundary conditions for the design of the detuning factor x_c, enabling the avoidance of bifurcation and achieving a full range of ZVS in systems with CRL or CVL. The comprehensive analysis conducted in this article provides valuable insights for designing high-performance IPT systems, particularly in terms of system parameter selection, operating regions, and controller design. The validity of the proposed comprehensive analysis is supported by experimental results.

REFERENCES

[1] S. Y. Hui, "Planar wireless charging technology for portable electronic products and Qi," *Proc. IEEE*, vol. 101, no. 6, pp. 1290–1301, Jun. 2013.

[2] S. Li and C. C. Mi, "Wireless power transfer for electric vehicle applications," *IEEE J. Emerg. Sel. Topics Power Electron.*, vol. 3, no. 1, pp. 4–17, Mar. 2015.

[3] G. Guidi, J. A. Suul, F. Jenset, and I. Sorfonn, "Wireless charging for ships: High-power inductive charging for battery electric and plug-in hybrid vessels," *IEEE Electrific. Mag.*, vol. 5, no. 3, pp. 22–32, Sep. 2017.

[4] C.-S. Wang, G. A. Covic, and O. H. Stielau, "Power transfer capability and bifurcation phenomena of loosely coupled inductive power transfer systems," *IEEE Trans. Ind. Electron.*, vol. 51, no. 1, pp. 148–157, Feb. 2004.

[5] U. Iruretagoyena, A. Garcia-Bediaga, L. Mir, H. Camblong, and I. Villar, "Bifurcation limits and non-idealities effects in a three-phase dynamic IPT system," *IEEE Trans. Power Electron.*, vol. 35, no. 1, pp. 208–219, Jan. 2020.

[6] J. Wu, K. Li, J. Zeng, and S.-Y. R. Hui, "On the limitations of the coupled mode theory and parity-time symmetry for near-field wireless power transfer research," *IEEE Trans. Power Electron.*, vol. 39, no. 5, pp. 6433–6441, May 2024.

[7] K. Aditya and S. S. Williamson, "Design guidelines to avoid bifurcation in a series–series compensated inductive power transfer system," *IEEE Trans. Ind. Electron.*, vol. 66, no. 5, pp. 3973–3982, May 2019.

[8] Y. Zhang and Z. Zhao, "Frequency splitting analysis of two-coil resonant wireless power transfer," *IEEE Antennas Wireless Propag. Lett.*, vol. 13, pp. 400–402, Feb. 2014.

[9] A. P. Sample, D. T. Meyer, and J. R. Smith, "Analysis, experimental results, and range adaptation of magnetically coupled resonators for wireless power transfer," *IEEE Trans. Ind. Electron.*, vol. 58, no. 2, pp. 544–554, Feb. 2011.

[10] W.-Q. Niu, J.-X. Chu, W. Gu, and A.-D. Shen, "Exact analysis of frequency splitting phenomena of contactless power transfer systems," *IEEE Trans. Circuits Syst. I, Reg. Papers*, vol. 60, no. 6, pp. 1670–1677, Jun. 2013.

[11] Y. Zhang, Z. Zhao, and K. Chen, "Frequency-splitting analysis of four-coil resonant wireless power transfer," *IEEE Trans. Ind. Appl.*, vol. 50, no. 4, pp. 2436–2445, Jul./Aug. 2014.

[12] X. Liu, X. Yuan, C. Xia, and X. Wu, "Analysis and utilization of the frequency splitting phenomenon in wireless power transfer systems," *IEEE Trans. Power Electron.*, vol. 36, no. 4, pp. 3840–3851, Apr. 2021.

[13] H. Nguyen and J. I. Agbinya, "Splitting frequency diversity in wireless power transmission," *IEEE Trans. Power Electron.*, vol. 30, no. 11, pp. 6088–6096, Nov. 2015.

[14] F. N. Esfahani, S. M. Madani, M. Niroomand, and A. Safaee, "Maximum wireless power transmission using real-time single iteration adaptive impedance matching," *IEEE Trans. Circuits Syst. I, Reg. Papers*, vol. 70, no. 9, pp. 3806–3817, Sep. 2023.

[15] Z. U. Zahid et al., "Design and control of a single-stage large air-gapped transformer isolated battery charger for wide-range output voltage for EV applications," in *Proc. IEEE Energy Convers. Congr. Expo.*, Denver, CO, USA, Sep. 2013, pp. 5481–5487.

[16] Y. Jiang, L. Wang, Y. Wang, J. Liu, M. Wu, and G. Ning, "Analysis, design, and implementation of WPT system for EV's battery charging based on optimal operation frequency range," *IEEE Trans. Power Electron.*, vol. 34, no. 7, pp. 6890–6905, Jul. 2019.

[17] Y. Frechter and A. Kuperman, "Output voltage range of a power loaded series–series compensated inductive wireless power transfer link operating in load-independent regime," *IEEE Trans. Power Electron.*, vol. 35, no. 6, pp. 6586–6593, Jun. 2020.

[18] G. Guidi and J. A. Suul, "Minimizing converter requirements of inductive power transfer systems with constant voltage load and variable coupling conditions," *IEEE Trans. Ind. Electron.*, vol. 63, no. 11, pp. 6835–6844, Nov. 2016.

[19] Y. Zhang, T. Kan, Z. Yan, and C. C. Mi, "Frequency and voltage tuning of series–series compensated wireless power transfer system to sustain rated power under various conditions," *IEEE J. Emerg. Sel. Topics Power Electron.*, vol. 7, no. 2, pp. 1311–1317, Jun. 2019.

[20] W. S. Burnside and A. W. Panton, *The Theory of Equations: With an Introduction to the Theory of Binary Algebraic Forms*. Ann Arbor, MI, USA: Univ. of Michigan Library, 1899.

[21] S. Fan, "A new extracting formula and a new distinguished means on the one valuable cubic equation," *Natural Sci. J. Hainan Teachers College*, vol. 2, pp. 91–98, 1989.

[22] C. Zheng et al., "High-efficiency contactless power transfer system for electric vehicle battery charging application," *IEEE J. Emerg. Sel. Topics Power Electron.*, vol. 3, no. 1, pp. 65–74, Mar. 2015.

[23] M. Chen and G. A. Rincon-Mora, "Accurate electrical battery model capable of predicting runtime and I-V performance," *IEEE Trans. Energy Convers.*, vol. 21, no. 2, pp. 504–511, Jun. 2006.

[24] T. Duerbaum, "First harmonic approximation including design constraints," in *Proc. 20th Int. Telecommun. Energy Conf.*, San Francisco, CA, USA, 1998, pp. 321–328.

[25] Z. Wei, B. Zhang, S. Lin, and C. Wang, "A self-oscillation WPT system with high misalignment tolerance," *IEEE Trans. Power Electron.*, vol. 39, no. 1, pp. 1870–1887, Jan. 2024.
[26] M. Kasper, R. M. Burkart, G. Deboy, and J. W. Kolar, "ZVS of power MOSFETs revisited," *IEEE Trans. Power Electron.*, vol. 31, no. 12, pp. 8063–8067, Dec. 2016.

Jiayu Zhou received the B.Eng. and M.S. degrees in electrical engineering from Beijing Jiaotong University, Beijing, China, in 2016 and 2019, respectively, and the Ph.D. degree in engineering cybernetics from the Norwegian University of Science and Technology, Trondheim, Norway, in 2023.

He was a Visiting Student with Tennessee Technological University, USA, and Nanyang Technological University, Singapore. His research interests include inductive power transfer and power converters for renewable energy system.

C. Q. Jiang (Senior Member, IEEE) received the B.Eng. and M.Eng. degrees (first class hons.) in electrical engineering and automation from Wuhan University, Wuhan, China, in 2012 and 2015, respectively, and the Ph.D. degree in electrical and electronic engineering from The University of Hong Kong, Hong Kong, in 2019.

He is currently an Assistant Professor with the Department of Electrical Engineering, Faculty Member with the State Key Laboratory of Terahertz and Millimeter Waves, City University of Hong Kong, Hong Kong. Since 2021, he has also been with Clare Hall, University of Cambridge. From 2019 to 2021, he was a Postdoctoral Research Associate with the University of Cambridge, Cambridge, U.K. In 2019, he was a Visiting Researcher with the Nanyang Technological University, Singapore. His research interests include power electronics, wireless power transfer techniques, electric machines and drives, and electric vehicle technologies.

Dr. Jiang was the recipient of Gold Medals with Congratulations of the Jury in International Exhibition of Inventions of Geneva, Winner of CAPE Acorn Blue Sky Research Award with the University of Cambridge, Gold Medal in Asia Exhibition of Innovations and Inventions, Silver Award and Bronze Award in Shenzhen Qianhai Youth Innovation and Entrepreneurship Competition, and First Prize in the Interdisciplinary Research Competition with the University of Hong Kong. He is currently an Associate Editor of *IET Renewable Power Generation*, Guest Editor of Energies, Electronics, Wireless Power Transfer, IEEE OPEN JOURNAL OF VEHICULAR TECHNOLOGY.

Tianlu Ma (Graduate Student Member, IEEE) received the B.Eng. degree in electrical engineering and automation from Jilin University, Changchun, China, in 2018, and the M.Sc. degree in electrical engineering from Xi'an Jiaotong University, Xi'an, China, in 2021. He is currently working toward the Ph.D. degree in electrical engineering with the City University of Hong Kong, Hong Kong.

His research interests include stationary and dynamic wireless power transfer modeling and control, coupler design, and power electronics.

Mr. Ma was the recipient of the Best Presentation Award and First Prize in the 2nd IEEE PELS Student Symposium on Power Electronics in Asia and the Gold Medal at the 49th International Exhibition of Inventions of Geneva.

Giuseppe Guidi (Senior Member, IEEE) received the Graduate degree in electrical engineering from the University of L'Aquila, L'Aquila, Italy, in 1995, and the Ph.D. degree in electric power engineering from the Norwegian University of Science and Technology (NTNU), Trondheim, Norway, in 2009.

He was involved in the field of power electronic drives from 1997 to 2004, joining first Fuji Electric R&D, Japan, as R&D Engineer and then SIEI SpA, Italy, as a Senior Engineer. In 2009, he was with Yokohama National University, Yokohama, Japan, as a Research Associate, working on power converters for electric vehicles. From 2011, he was a part-time Research Associate with NTNU, until joining SINTEF Energy Research, Trondheim, Norway, in 2013. His current research interests include power electronics, traction control, and drive systems for electric propulsion, as well as application of power electronics to renewable energy.

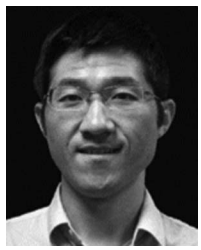

Xinan Zhang (Senior Member, IEEE) received the B.E. degree in electrical engineering and automation from Fudan University, Shanghai, China, in 2008, and the Ph.D. degree in electrical engineering from Nanyang Technological University (NTU), Singapore, in 2014.

He was a Postdoctoral Researcher with NTU and the University of New South Wales from 2014 to 2017. From 2017 to 2019, he was a Lecturer with NTU. In 2019, he was with the University of Western Australia, Perth, WA, Australia, where he is currently an Associate Professor. His research interests include electrical machine drives, control and modulation of power electronic converters, and management of hybrid energy storage systems.

Jon Are Suul (Member, IEEE) received the M.Sc. degree in energy and environmental engineering and the Ph.D. degree in electric power engineering from the Norwegian University of Science and Technology (NTNU), Trondheim, Norway, in 2006 and 2012, respectively.

From 2006 to 2007, he was with SINTEF Energy Research, Trondheim, where he was working with simulation of power electronic converters and marine propulsion systems until starting his Ph.D. studies. Since 2012, he has been a Research Scientist with SINTEF Energy Research, first in a part-time position while working as a part-time Postdoctoral Researcher with the Department of Electric Power Engineering, NTNU, until 2016. Since 2017, he has been an Adjunct Associate Professor with the Department of Engineering Cybernetics, NTNU. His research interests include modeling, analysis, and control of power electronic converters in power systems, renewable energy applications, and electrification of transport.

Dr. Suul is an Editor of IEEE JOURNAL OF EMERGING AND SELECTED TOPICS IN POWER ELECTRONICS and an Associate Editor for IEEE TRANSACTIONS ON ENERGY CONVERSION and *Journal of Emerging and Selected Topics in Industrial Electronics*.